



A redox-flow battery with an alloxazine-based organic electrolyte

Citation

Lin, Kaixiang, Rafael Gómez-Bombarelli, Eugene S. Beh, Liuchuan Tong, Qing Chen, Alvaro Valle, Alán Aspuru-Guzik, Michael J. Aziz, and Roy G. Gordon. 2016. "A Redox-Flow Battery with an Alloxazine-Based Organic Electrolyte." *Nature Energy* 1 (9) (July 18): 16102. doi:10.1038/nenergy.2016.102.

Published Version

10.1038/nenergy.2016.102

Permanent link

<http://nrs.harvard.edu/urn-3:HUL.InstRepos:33439113>

Terms of Use

This article was downloaded from Harvard University's DASH repository, and is made available under the terms and conditions applicable to Open Access Policy Articles, as set forth at <http://nrs.harvard.edu/urn-3:HUL.InstRepos:dash.current.terms-of-use#OAP>

Share Your Story

The Harvard community has made this article openly available.
Please share how this access benefits you. [Submit a story](#).

[Accessibility](#)

1 **A redox flow battery with an alloxazine-based organic electrolyte**

2 **Kaixiang Lin¹, Rafael Gómez-Bombarelli¹, Eugene S. Beh^{1,2}, Liuchuan Tong¹, Qing**
3 **Chen², Alvaro Valle³, Alán Aspuru-Guzik¹, Roy G. Gordon^{1,2*}, Michael J. Aziz^{2*}**

4 ¹ *Department of Chemistry and Chemical Biology, Harvard University, 12 Oxford*
5 *Street, Cambridge, Massachusetts 02138, USA*

6 ² *Harvard John A. Paulson School of Engineering and Applied Sciences, 29 Oxford*
7 *Street, Cambridge, Massachusetts 02138, USA*

8 ³ *Harvard College, Cambridge, Massachusetts 02138, USA*

9 *E-mail: RGG (gordon@chemistry.harvard.edu) and MJA (aziz@seas.harvard.edu)

10

11 **Redox flow batteries (RFBs) can store large amounts of electrical energy**
12 **from variable sources, such as solar and wind. Recently, redox-active organic**
13 **molecules in aqueous RFBs have drawn substantial attention due to their rapid**
14 **kinetics and low membrane crossover rates. Drawing inspiration from nature, here**
15 **we report a high-performance aqueous RFB utilizing an organic redox compound,**
16 **alloxazine, which is a tautomer of vitamin B₂'s isoalloxazine backbone. It can be**
17 **synthesized in high yield at room temperature by single-step coupling of inexpensive**
18 ***o*-phenylenediamine derivatives and alloxan. The highly alkaline-soluble alloxazine**
19 **7/8-carboxylic acid (ACA) produces a RFB exhibiting open-circuit voltage**
20 **approaching 1.2 volts and current efficiency and capacity retention exceeding 99.7%**
21 **and 99.98% per cycle, respectively. Theoretical studies indicate that structural**
22 **modification of alloxazine with electron donating groups should allow further**

23 **increases in battery voltage. As an aza-aromatic molecule that undergoes reversible**
24 **redox cycling in aqueous electrolyte, alloxazine represents a class of radical-free**
25 **redox-active organics for use in large-scale energy storage.**

26 Improved methods for storing electrical energy from intermittent renewable
27 sources are needed to support the rapid deployment of photovoltaic (PV) and wind
28 power.¹⁻³ A promising approach for safe and cost-effective stationary energy storage uses
29 redox flow batteries (RFBs), in which the energy is stored in fluids held outside the
30 power conversion electrochemical cell.^{4,5} This permits the independent engineering of
31 energy (electrolyte volume and/or concentration) and power (cell area) capacities and
32 enables the attainment of the high energy-to-power ratios (i.e. long discharge durations at
33 rated power) necessary to deliver energy from PV and wind when it is needed. Since the
34 invention of RFBs in the 1970s, the development efforts for its electrolyte materials – the
35 core component of RFBs – have concentrated on single metal ions such as vanadium,
36 iron and chromium, where the battery voltages are fixed by the reduction potentials of
37 these ions, and their solubilities and stabilities are governed by the pH and composition
38 of the supporting electrolyte.^{6,7} However, their development has been impeded by one or
39 more shortcomings such as high electrolyte corrosivity, toxicity, cost, membrane cross-
40 over rate, or sluggish reaction kinetics.

41 Contrary to the limited numbers of metal ions suitable for RFBs, organic
42 molecules display high chemical diversity, allowing optimization of electrolyte properties
43 such as higher solubility (by adding solubilizing groups), higher voltage (by varying the
44 electron donating properties of functional groups), and lower membrane cross-over rate
45 (by tuning the molecular size or net charge on the molecules). Recently, researchers have

46 demonstrated RFBs of much improved performance by rational design of organic-based
47 electrolyte materials (summarized in Table 1).⁸⁻¹³ For instance, Huskinson *et al.* utilized a
48 sulfonic-acid functionalized 9,10-anthraquinone, which showed fast kinetics and high
49 solubility in a supporting electrolyte of sulfuric acid; by pairing it up with cheap
50 bromine/hydrobromic acid, the team showed approximately a three-fold reduction of the
51 potential cost of electrolyte materials, compared with state-of-art all-vanadium RFBs.^{8,9}
52 The toxicity and corrosivity of bromine, however, limit its use to industrial and utility
53 settings. By switching from acidic to alkaline supporting electrolyte, Lin *et al.*
54 demonstrated a less corrosive and non-toxic RFB using hydroxylated 9,10-anthraquinone
55 and a food additive, ferrocyanide, targeted for residential and commercial usage.¹⁰ To
56 reduce membrane cost while maintaining a low membrane crossover rate, Janoschka *et*
57 *al.* prepared polymeric methyl viologen and (2,2,6,6-tetramethylpiperidin-1-yl)oxidanyl
58 (TEMPO) which showed almost no sign of membrane crossover when cheap dialysis
59 membranes were used in place of expensive cation-exchange membranes.¹¹ Despite these
60 great advances, each system still has potential for further improvement, such as replacing
61 toxic halogen species with high-performance organic molecules, increasing the ion
62 conductivity and energy density of alkaline systems, and reducing the high electrolyte
63 viscosity associated with the dissolution of polymers at practical concentrations. To
64 accelerate the development of organic-based RFBs, more compounds with useful redox
65 potential, high solubility, and ease of synthesis are highly desired. Previous aqueous
66 organic-based RFBs have utilized only three types of stable redox-active species: **1)**
67 **quinones, 2) TEMPO and 3) methyl viologen**, as shown in Table 1. To date, tailored
68 improvements have been proven possible only in quinone systems.

69 Gaining inspiration from naturally occurring flavin cofactors, here we report a
70 novel alloxazine-based aqueous organic RFB. Alloxazines can be synthesized via a
71 simple and high-yielding coupling reaction between *o*-phenylenediamine derivatives and
72 alloxan in acetic acid and boric acid at room temperature and atmospheric pressure
73 (Table 2).^{14–16} Functionalization of alloxazine with a carboxylic acid group renders the
74 alloxazine molecule highly soluble in alkaline solution – up to 2 M in pH 14 KOH, which
75 corresponds to a charge density of 108 Ah/L. By pairing it up with ferri/ferrocyanide as
76 the positive electrolyte, we built a high-performance RFB characterized by an open-
77 circuit voltage approaching 1.2 V and current efficiency and capacity retention exceeding
78 99.7% and 99.98% per cycle, respectively. Enabled by a high-throughput computational
79 study, a relationship between different alloxazine functional groups and their effects on
80 reduction potential was established and exploited to guide the design of future alloxazine-
81 based electrolyte materials. For instance, by replacing the carboxylic acid group with
82 another alkaline-soluble hydroxyl group, the battery voltage can be further raised by
83 almost 10%.

84 **Rational Design of Electrolyte Material**

85 Designing an appropriate organic molecule as electrolyte material starts from
86 identifying redox-active cores followed by functionalization of the core structure to
87 achieve a practical reduction potential and solubility. We observed that riboflavin 5'
88 phosphate (FMN), a highly water-soluble compound derived from vitamin B₂, undergoes
89 two-electron reduction *via* a flavin semiquinone radical intermediate on its isoalloxazine
90 backbone (Supplementary Fig. 1).^{17,18} In alkaline solution, it exhibited high reversibility
91 and a low reduction potential of –0.53 V vs. SHE (Fig. 1a). Further exploration of its

92 isoalloxazine motif led to the discovery that lumichrome, an alloxazine derivative that
93 differs from isoalloxazine by its diazabutadiene double bond configuration, exhibited a
94 much lower reduction potential of -0.70 V vs. SHE (Fig. 1b). Alloxazine had previously
95 been studied in the solid state as an anode material for non-aqueous lithium and sodium
96 ion batteries.¹⁹ However, the low solubility of alloxazine in a wide range of solvents
97 presents a challenge for solution-phase applications. To increase its solubility in aqueous
98 solution, we functionalized the alloxazine core with an alkali-soluble carboxylic acid
99 group by coupling *o*-phenylenediamine-4-carboxylic acid (a.k.a. 3,4-diaminobenzoic acid)
100 with alloxan to afford an isomeric mixture of alloxazine 7/8-carboxylic acid (ACA) in
101 almost 100% yield (Supplementary Fig. 2). The reduction potential of ACA from CV
102 measurement is -0.62 V vs. SHE (Fig. 1c). The larger separation between its oxidation
103 and reduction peaks than those of FMN and lumichrome is likely due to slower kinetics.
104 From our rotating disk electrode (RDE) measurement, the reduction rate constant was
105 measured to be $1.2 \pm 0.2 \times 10^{-5}$ cm s⁻¹ (Supplementary Fig. 3). Nevertheless, this value is
106 still an order of magnitude higher than that of the slower side of all-vanadium RFBs.⁶

107 Besides the large shift in reduction potential moving from isoalloxazine to
108 alloxazine, we also observed a significant increase in chemical stability in alkaline
109 conditions. Whereas cyclic voltammetry (CV) measurement of 0.5 M FMN in an alkaline
110 solution revealed an almost 70% decrease in reduction signal within 2 weeks, an ACA
111 solution at the same concentration showed almost no sign of degradation (Supplementary
112 Fig. 4). Quantification of ACA stability was achieved by proton nuclear magnetic
113 resonance (¹H NMR) analysis of a 0.5 M solution of ACA maintained at pH 14 over the
114 course of six weeks. The decomposition of ACA, assuming first-order kinetics ($R^2 =$

115 0.991), had a rate constant of $1.39 \times 10^{-3} \text{ day}^{-1}$, equivalent to a solution half-life of 500
116 days (Supplementary Fig. 5). This combination of lower reduction potential (-0.62 V vs.
117 -0.53 V) and higher chemical stability (500 days vs. 10 days half-life of FMN at pH 14),
118 made ACA a much better candidate for an electrolyte material.

119 **Electrochemical Full-cell Study**

120 To demonstrate ACA in a full cell, we paired ACA with ferri/ferrocyanide (Fig.
121 1c and d). The battery was assembled using 0.5 M ACA (1.5 mmol) as the negative
122 electrolyte and 0.4 M ferrocyanide (4.5 mmol) + 40 mM ferricyanide (0.46 mmol) as the
123 positive electrolyte. Both solutions were adjusted to pH 14 by KOH. Excess quantities of
124 ferrocyanide and ferricyanide were used to ensure the negative terminal remained the
125 capacity-limiting side for the purpose of evaluating its electrochemical stability during
126 cycling. The resulting alkaline aqueous RFB showed an open-circuit voltage (OCV)
127 approaching 1.2 V. The OCV versus state-of-charge (SOC) monotonically increased from
128 10% to 90% SOC (Fig 2a). Polarization studies conducted at room temperature showed a
129 peak power density of 0.35 W cm^{-2} at a current density of 0.58 A cm^{-2} . The linearity of
130 the polarization curves allows us to derive a polarization area-specific resistance (ASR),
131 which is $1.03 \Omega \text{ cm}^2$ at 50% SOC. About 70% of this cell ASR is contributed by the
132 membrane (Supplementary Fig. 6), similar to our previous observation.¹⁰ Note that ACA
133 redox kinetics does not show up as a significant kinetic overvoltage loss (i.e. a non-
134 linearity at the low overvoltage region) in the polarization curve, likely owing to the large
135 surface area provided by the porous carbon electrodes. The electrochemical stability of
136 ACA was evaluated based on an extended charge-discharge study over 400 cycles (Fig.
137 2c). The current efficiency exceeded 99.7% at 0.1 A cm^{-2} , which is indicative of

138 negligible side reactions during cell cycling and a low crossover rate through the
139 membrane. The round-trip energy efficiency in this cycling experiment averaged around
140 63%. The battery exhibited a remarkably high capacity retention rate of more than 91%
141 over 400 cycles, or a capacity loss rate of 0.023% per cycle. To further analyze capacity
142 retention, we compared the total charge from the cell before and after cycling using
143 chronoamperometry to charge and discharge the cell at constant voltage (Supplementary
144 Fig. 7). From this result, the measured capacity retention from 400 cycles was 95%, i.e.
145 the loss rate was 0.013% per cycle. We believe the discrepancy between this
146 measurement and the capacity retention observed during constant-current cycling was
147 due to an increase of system resistance (which we infer from decreasing energy
148 efficiency with cycle number); this effect moved the charging and discharging curves
149 closer to the cutoff voltages, resulting in less complete charging and discharging with
150 increasing cycle count (Supplementary Fig. 8). We expect further cell development,
151 including variations in pH, membrane and sealing method, to lead to further improvement
152 of capacity retention. By increasing the concentration of ACA to 1 M, we increased the
153 electrolyte charge density by almost two-fold (Supplementary Fig. 9a). Together with
154 adjusted cell compression and higher ACA concentration, we were able to improve
155 round-trip energy efficiency to 74%, while retaining the same level of current efficiency
156 (99.7%) and capacity retention per cycle (99.95%) (Supplementary Fig. 9b).

157 **Theoretical Modeling and Screening**

158 One useful feature of organic electrolyte materials is the ability to optimize their
159 properties through chemical modification, a process that can be accelerated by virtual
160 testing with computational methods.^{8,20} We assayed the chemical landscape around the

161 alloxazine backbone by computing the properties of derivatives bearing one to four
162 copies of each of seven functional groups. Selected examples of alloxazine derivatives
163 subjected to the theoretical modeling are shown in Table 3 (a complete table of the rest of
164 the studied alloxazine derivatives can be found in supplementary table 1).

165 Figure 3 shows the variation in predicted standard reduction potential (E^0) within
166 the alloxazine class. The additive effect of electron donating and electron withdrawing
167 groups is observed as they lower and raise the reduction potential, respectively, across a
168 range of 400 mV. Hydroxyl, methyl and methoxy substituents afford the largest increases
169 in cell potential. We prepared 7/8-hydroxyalloxazine and 7,8-dimethylalloxazine via the
170 aforementioned *o*-phenylenediamine-alloxan coupling chemistry (Table 2,
171 Supplementary Fig. 10 and 11). CV of these two compounds showed values below
172 -0.73 V (~ 110 mV lower than ACA), potentially raising the battery voltage by another
173 10% (Fig 3c and d).

174 In addition to tuning its reduction potential, modification of alloxazine with
175 appropriate functional groups could also improve its chemical stability. Alloxazines
176 undergo ring-opening reaction in aqueous solvent via addition of water to the amidic
177 carbonyls followed by continuing hydrolysis to redox-inactive species (Supplementary
178 Fig. 12).²¹ Increases in pH catalyze the hydrolysis process, as observed in the FMN
179 stability study and informed by literature.^{22,23} Nevertheless, the low pK_a values at the
180 amide nitrogen (8.4 and 11.4 for lumichrome²⁴) result in the accumulation of two
181 negative charges in the imidic conjugate system at high pH values; this process ultimately
182 hinders the hydrolysis reaction by lowering the electrophilicity of the carbonyl groups.²⁵
183 Since the redox center and the center of electrophilic reactivity are separate in alloxazines,

184 design strategies are available to decrease chemical reactivity, such as tuning the
185 electrophilicity of alloxazines via different functional groups. We evaluated all the
186 screened alloxazines based on their predicted equilibrium constant, K_{hyd} , for the
187 reversible hydration of the carbonyl groups (Fig. 3b), with lower value of K_{hyd}
188 corresponding to less electrophilic carbonyls. We found that the same electron-donating
189 groups that contribute toward the desired reduction potential values also have a protecting
190 effect against hydrolysis, as is the case with amides in general (i.e. hydrolysis rate of
191 amides in basic medium has a linear dependence in K_{hyd}).²⁶ For instance, hydroxyl
192 derivatives lower K_{hyd} by as much as two orders of magnitude, thereby shifting the
193 equilibrium toward the redox-active “de-hydrated” form.

194 **Conclusions**

195 By drawing inspiration from vitamin B₂, we introduced a novel family of organic
196 molecules for RFB applications. The alloxazine redox-center exhibits sufficiently high
197 electrochemical and chemical stability, and sufficiently low reduction potential, to be
198 exploited as a negative electrolyte material in an alkaline RFB. Synthesis of a
199 functionalized alloxazine redox-active center was carried out via a very simple coupling
200 chemistry utilizing only *o*-phenylenediamine derivatives, alloxan, acetic acid and boric
201 acid, without employing high temperature or pressure. We paired alloxazine 7/8-
202 carboxylic acid with ferri/ferrocyanide to demonstrate a high-performance alloxazine-
203 powered RFB. The current efficiency exceeded 99.7% while its capacity retention over
204 400 charge-discharge cycles was shown to be ~95% cumulatively, or 99.98% per cycle.
205 With a better understanding of the alloxazine system enabled by theoretical modeling, we
206 have designed and characterized another two alloxazine-derived molecules promising

207 almost 10% further increase in battery voltage. The introduction of aza-aromatic redox-
208 active species opens up a new direction in designing organic electrolyte and delivers a
209 promising pathway to accelerate development of aqueous organic RFBs.

210 **Methods**

211 **Chemical synthesis and characterization** 3,4-diaminophenol was purchased from Aurum Pharmatech and
212 used as received. All other chemicals were purchased from Sigma Aldrich and used as received.

213 Alloxazines were prepared following previously reported methods.¹⁴⁻¹⁶ In general, *o*-phenylenediamine (5
214 mmol) was added to 45 mL acetic acid followed by alloxan (5.5 mmol) and boric acid (5.5 mmol). The
215 reaction mixture was stirred at room temperature and atmospheric pressure under nitrogen. The reaction
216 times for various alloxazine derivatives are summarized in Table 2. After reaction, the product was
217 collected by vacuum filtration, washed with acetic acid, water, and diethyl ether, and air dried overnight.
218 The products were analyzed by ¹H NMR and used for chemical and electrochemical measurement without
219 further purification. ¹H NMR spectra were recorded using Varian INOVA 500 (500 MHz) NMR
220 spectrometers at 23 °C. Proton chemical shifts are expressed in parts per million (ppm, δ scale) and are
221 referenced to residual protium in the NMR solvent (D₂O, δ 4.80 ppm and (CD₃)₂SO, δ 2.50 ppm). The
222 isomeric ratio between major and minor product during the preparation of ACA and 7/8-hydroxyalloxazine
223 was estimated based on their peak integration ratio (highlighted in Supplementary Fig. 2 and 10).

224 **Stability test by ¹H NMR** In a nitrogen-filled glove bag, a sample of ACA (0.5 M) was dissolved in a
225 solution of 40% wt. KOD in D₂O (used as received from Sigma-Aldrich) which was then adjusted to pH 14
226 with the appropriate amount of D₂O. The sample was sealed inside a J. Young tube and analyzed by ¹H
227 NMR. Analyses of the same sample were performed after 14, 21, 28, and 42 days. Between analyses, the J.
228 Young tube was returned to the glove bag where it was kept in the dark. The proportion of ACA that had
229 decomposed was determined by integrating the peaks at 6.48 ppm and comparing it to the peaks at 6.60
230 ppm and 6.86 ppm, which come from the starting material. From this data, the rate constant of ACA
231 decomposition was calculated assuming first-order kinetics (Supplementary Fig. 4).

232 **Solubility measurement by UV-Vis spectroscopy** Saturated solution of ACA was prepared by addition of
233 ACA to a pH 14 solution until precipitate formed. KOH was added if necessary to maintain the solution pH.
234 Aliquots of the supernatant were diluted with a pH 14 KOH solution and its absorbance measured using
235 UV-Vis spectrophotometry (Ocean Optics FLAME-S-UV-VIS; cuvettes are made out of polystyrene with a

236 path length of 1 cm). Readings were interpolated based on a standard calibration curve prepared by
237 measuring the absorbance of known concentrations of ACA (Supplementary Fig. 13).

238 **Electrochemical analysis** Three-electrode cyclic voltammetry tests (CV) were performed using a glassy
239 carbon working electrode, a Ag/AgCl reference electrode (pre-soaked in 3 M NaCl solution) and a
240 platinum counter electrode. For the full cell measurements, cell hardware from Fuel Cell Tech.
241 (Albuquerque, NM) was used to assemble a zero-gap flow cell configuration, similar to previous reports.²⁷
242 POCO graphite flow plates with serpentine flow fields were used for both sides. A 5 cm² geometric surface
243 area electrode comprised a stack of two or three sheets of Sigracet SGL 10AA porous carbon paper,
244 pretreated by baking in air at 400 °C for 24 h. A sheet of Nafion 212 membrane, pretreated in DI water
245 overnight, served as the ion-selective membrane. The rest of the space between the plates was gasketed by
246 either Kalrez or Teflon sheets. The electrolytes were fed into the cell through PFA tubing, at a rate of 60
247 mL/min controlled by Cole-Parmer Masterflex L/S peristaltic pumps. All electrochemical tests were
248 performed using a Gamry Reference 3000 potentiostat.

249 **Rotating disk electrode (RDE) measurement** RDE experiments were conducted using a BASi RDE
250 (RDE-2) instrument equipped with a glassy carbon working electrode, a Ag/AgCl reference electrode (pre-
251 soaked in 3 M NaCl solution) and a platinum counter electrode. The electrode was rotated at a specific
252 speed while the voltage was linearly swept from -0.70 V to -1.20 V versus Ag/AgCl. The reduction rate
253 constant of ACA was calculated from the Tafel equation using the following parameters: $n = 2$; Faraday's
254 constant $F = 96,485 \text{ C mol}^{-1}$; electrode area $A = 0.0707 \text{ cm}^2$, ACA concentration $C = 2 \times 10^{-6} \text{ mol cm}^{-3}$;
255 kinematic viscosity $\nu = 0.01 \text{ cm}^2 \text{ s}^{-1}$ (Supplementary Fig. 3). The experiment was performed three times.

256 **Electrolyte preparation** For SOC, polarization and 400-cycle charge-discharge studies, the positive
257 electrolyte was prepared by dissolving ferrocyanide (1.9 g, 4.5 mmol) and ferricyanide (0.15 g, 0.46 mmol)
258 in 1 M KOH solution (11.25 mL) to afford 0.4 molar electron concentration and 2.7 molar K⁺ ion solution
259 (11 Ah/L charge density). The negative electrolyte was prepared by dissolving ACA (0.39 g, 1.5 mmol) in
260 2.5 M KOH solution (adjusted to final volume of 3 mL) to afford 1 molar electron concentration and 2
261 molar K⁺ ion solution (27 Ah/L charge density). For high concentration ACA cycling experiment, the
262 positive electrolyte was prepared by dissolving ferrocyanide (3.8 g, 9 mmol) and ferricyanide (0.3 g, 0.91

263 mmol) in 1 M KOH solution (22.5 mL) to afford 0.4 molar electron concentration and 2.7 molar K^+ ion
264 solution (11 Ah/L charge density). The negative electrolyte was prepared by dissolving ACA (0.78 g, 3
265 mmol) in 4 M KOH solution (adjusted to final volume of 3 mL) to afford 2 molar electron concentration
266 and 4 molar K^+ ion solution (54 Ah/L charge density).

267 **Computational studies**

268 *Libraries considered.* We have analyzed all the possible substitutions for each functional group on all the
269 possible sites of the alloxazine core. The functional groups assessed are carboxylic acid, fluoro, hydroxyl,
270 methoxy, methyl, phosphonic acid and sulfonic acid. Substitution on the alloxazine amide nitrogens were
271 not considered as they destabilize alloxazines under alkaline condition. A total of 105 backbones were
272 analyzed. Initial conformations were generated that used a random-distance matrix approach at the mmff94
273 level of theory. Geometries were further refined using DFT and single-point calculations were performed
274 using larger basis sets and solvent corrections. The following methods were tested for obtaining
275 equilibrium geometries and total energies: PM7, PM7 + implicit COSMO solvation, PBE/6-31G*,
276 B3LYP/6-31G*. In addition, single point calculations were performed at both B3LYP/6-311+G(d,p) and
277 B3LYP/6-311+G(d,p) combined with CPCM implicit solvation. Their relative performance is compared in
278 the supplementary information file. For both target properties we obtained the smallest error using
279 B3LYP/6-311+G(d,p) CPCM. Reduction potentials were predicted from the energy difference between the
280 reduced and oxidized forms of alloxazines, assuming a two-electron two-proton process. Prior to
281 conducting predictions, we assessed the performance of various quantum chemical methods to calculate the
282 two-proton two-electron redox potential of alloxazine and isalloxazine rings at $pH = 7.4$ using a
283 calibration scheme analogous to the one reported for quinones. The calibration dataset was composed of 23
284 experimentally-reported molecules, with $E^0_{pH=7}$ ranging between -380 meV and -80 meV versus RHE.²⁸
285 Our results suggest that quick semiempirical methods and gas-phase DFT calculations afford results with
286 mean errors around 20 meV. DFT calculations in implicit solvent with a larger basis set reduce the average
287 error to under 10 meV. The performance of various methods is reported in Supplementary Table 2. We then
288 corrected E^0 values to $pH = 14.0$. Pourbaix diagrams were estimated combining experimental and predicted
289 pK_a values ($pK_a^{ox} = 8.3, 11.4$; $pK_a^{red} = 6.7, 10.0$). The shift from $pH = 7.4$ to $pH = 14.0$ for alloxazines is

290 thus estimated at -320 meV. To calculate hydration equilibrium, we used an experimental dataset from the
291 literature including aldehydes, ketones, esters and amides and mapped theoretical reaction energies at 0 K
292 to experimentally-determined hydration equilibrium constants in water.²⁹ The calibration dataset was
293 composed of 41 experimentally-reported molecules, with $\log K_{\text{hyd}}$ ranging between -15 and 5 . DFT
294 calculations in implicit solvent result in mean errors close to 1 log unit. The performance of various
295 methods is reported in Supplementary Table 2.

296 **References**

- 297 1. Dunn, B., Kamath, H. & Tarascon, J.-M. Electrical Energy Storage for the Grid: A
298 Battery of Choices. *Science* **334**, 928–935 (2011).
- 299 2. Nguyen, T. & Savinell, R. F. Flow Batteries. *Electrochem. Soc. Interface* **19**, 54–56
300 (2010).
- 301 3. Yang, Z. *et al.* Electrochemical Energy Storage for Green Grid. *Chem. Rev.* **111**,
302 3577–3613 (2011).
- 303 4. Biello, D. Solar Wars. *Sci. Am.* **311**, 66–71 (2014).
- 304 5. Skyllas-Kazacos, M., Chakrabarti, M. H., Hajimolana, S. A., Mjalli, F. S. & Saleem,
305 M. Progress in Flow Battery Research and Development. *J. Electrochem. Soc.* **158**,
306 R55–R79 (2011).
- 307 6. Weber, A. Z. *et al.* Redox flow batteries: a review. *Journal of Applied*
308 *Electrochemistry* **41**, 1137–1164 (2011).
- 309 7. Perry, M. L. & Weber, A. Z. Advanced Redox-Flow Batteries: A Perspective. *J.*
310 *Electrochem. Soc.* **163**, A5064–A5067 (2016).
- 311 8. Huskinson, B. *et al.* A metal-free organic-inorganic aqueous flow battery. *Nature* **505**,
312 195–198 (2014).
- 313 9. Huskinson, B., Marshak, M. P., Gerhardt, M. R. & Aziz, M. J. Cycling of a Quinone-
314 Bromide Flow Battery for Large-Scale Electrochemical Energy Storage. *ECS Trans.*
315 **61**, 27–30 (2014).
- 316 10. Lin, K. *et al.* Alkaline quinone flow battery. *Science* **349**, 1529–1532 (2015).
- 317 11. Janoschka, T. *et al.* An aqueous, polymer-based redox-flow battery using non-
318 corrosive, safe, and low-cost materials. *Nature* **527**, 78–81 (2015).

- 319 12. Schubert, U. S. *et al.* Polymer/Zinc Hybrid-Flow Battery Using Block Copolymer
320 Micelles featuring a TEMPO Corona as Catholyte. *Polym Chem* **28**, 2238-2243 (2016).
- 321 13. Liu, T., Wei, X., Nie, Z., Sprenkle, V. & Wang, W. A Total Organic Aqueous Redox
322 Flow Battery Employing a Low Cost and Sustainable Methyl Viologen Anolyte and 4-
323 HO-TEMPO Catholyte. *Adv. Energy Mater.* **6**, 1501449 (2015).
- 324 14. Chen, S., Hossain, M. S. & Foss, F. W. Organocatalytic Dakin Oxidation by
325 Nucleophilic Flavin Catalysts. *Org. Lett.* **14**, 2806–2809 (2012).
- 326 15. Gonzalo, G. de, Smit, C., Jin, J., Minnaard, A. J. & Fraaije, M. W. Turning a
327 riboflavin-binding protein into a self-sufficient monooxygenase by cofactor redesign.
328 *Chem. Commun.* **47**, 11050–11052 (2011).
- 329 16. Lindén, A. A., Johansson, M., Hermanns, N. & Bäckvall, J.-E. Efficient and Selective
330 Sulfoxidation by Hydrogen Peroxide, Using a Recyclable Flavin–[BMIm]PF₆
331 Catalytic System. *J. Org. Chem.* **71**, 3849–3853 (2006).
- 332 17. Hasford, J. J. & Rizzo, C. J. Linear Free Energy Substituent Effect on Flavin Redox
333 Chemistry. *J. Am. Chem. Soc.* **120**, 2251–2255 (1998).
- 334 18. Müller, F. in *Radicals in Biochemistry* 71–107 (Springer, 1983).
- 335 19. Hong, J. *et al.* Biologically inspired pteridine redox centres for rechargeable batteries.
336 *Nat. Commun.* **5**, (2014).
- 337 20. Er, S., Suh, C., Marshak, M. P. & Aspuru-Guzik, A. Computational design of
338 molecules for an all-quinone redox flow battery. *Chem Sci* **6**, 885–893 (2015).
- 339 21. Koziol, J. & Metzler, D. E. Formation and Possible Structure of Covalent Hydrates of
340 Alloxazines. *Z. Für Naturforschung B* **27**, 1027–1029 (2014).

- 341 22. Surrey, A. R. & Nachod, F. C. Alkaline Hydrolysis of Riboflavin. *J. Am. Chem. Soc.*
342 **73**, 2336–2338 (1951).
- 343 23. Ahmad, I., Rapson, H. D. C., Heelis, P. F. & Phillips, G. O. Alkaline hydrolysis of
344 7,8-dimethyl-10-(formylmethyl)isoalloxazine. A kinetic study. *J. Org. Chem.* **45**, 731–
345 733 (1980).
- 346 24. Prukała, D. *et al.* Acid–Base Equilibriums of Lumichrome and its 1-Methyl, 3-Methyl,
347 and 1,3-Dimethyl Derivatives. *J. Phys. Chem. A* **116**, 7474–7490 (2012).
- 348 25. Koziol, J., Tyrakowska, B. & Müller, F. The structure of covalent hydrates of
349 alloxazines. A reinvestigation. *Helv. Chim. Acta* **64**, 1812–1817 (1981).
- 350 26. O’Connor, C. Acidic and basic amide hydrolysis. *Q. Rev. Chem. Soc.* **24**, 553–564
351 (1970).
- 352 27. Liu, Q. H. *et al.* High Performance Vanadium Redox Flow Batteries with Optimized
353 Electrode Configuration and Membrane Selection. *J. Electrochem. Soc.* **159**, A1246–
354 A1252 (2012).
- 355 28. Li, X.-L. & Fu, Y. Theoretical study of reduction potentials of substituted flavins. *J.*
356 *Mol. Struct. THEOCHEM* **856**, 112–118 (2008).
- 357 29. Gómez-Bombarelli, R., González-Pérez, M., Pérez-Prior, M. T., Calle, E. & Casado, J.
358 Computational Calculation of Equilibrium Constants: Addition to Carbonyl
359 Compounds. *J. Phys. Chem. A* **113**, 11423–11428 (2009).
- 360
- 361

362 **Acknowledgements**

363 This work was funded by the U.S. DOE ARPA-E award # DE-AR0000348, NSF # NSF-
364 CBET-1509041, the Massachusetts Clean Energy Technology Center and the Harvard
365 John A. Paulson School of Engineering and Applied Sciences. RGB and A A-G
366 acknowledge the use of the Harvard FAS Odyssey Cluster and support from FAS
367 Research Computing. We thank Chenxi Qian for designing the Figure 1d scheme.

368 **Author Contributions**

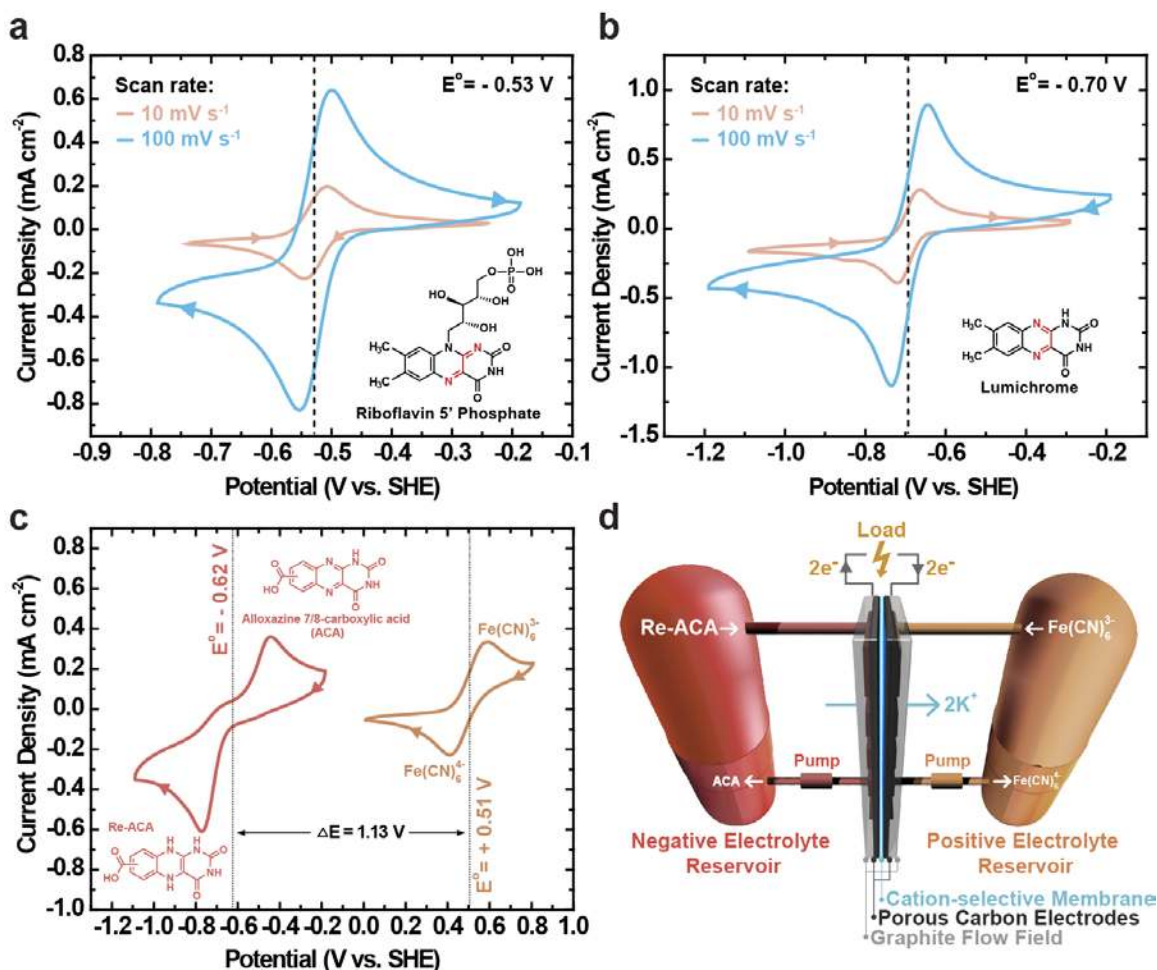
369 K.L., R.G.G. and M.J.A. formulated the project. K.L., and L.T. synthesized the
370 compounds. K.L., E.S.B. and L.T. collected and analyzed the NMR data. K.L., Q.C.,
371 E.S.B. and A.V. collected and analyzed the electrochemical data. K.L. and A.V.
372 measured solubility. R.G.B. and A.A.-G. performed theoretical analysis. K.L., R.G.G.
373 and M.J.A. wrote the paper, and all authors contributed to revising the paper.

374 **Additional Information**

375 Supplementary information is available online. Reprints and permissions information is
376 available online at www.nature.com/reprints. Correspondence and requests for materials
377 should be addressed to R.G.G and M.J.A.

378 **Competing interests**

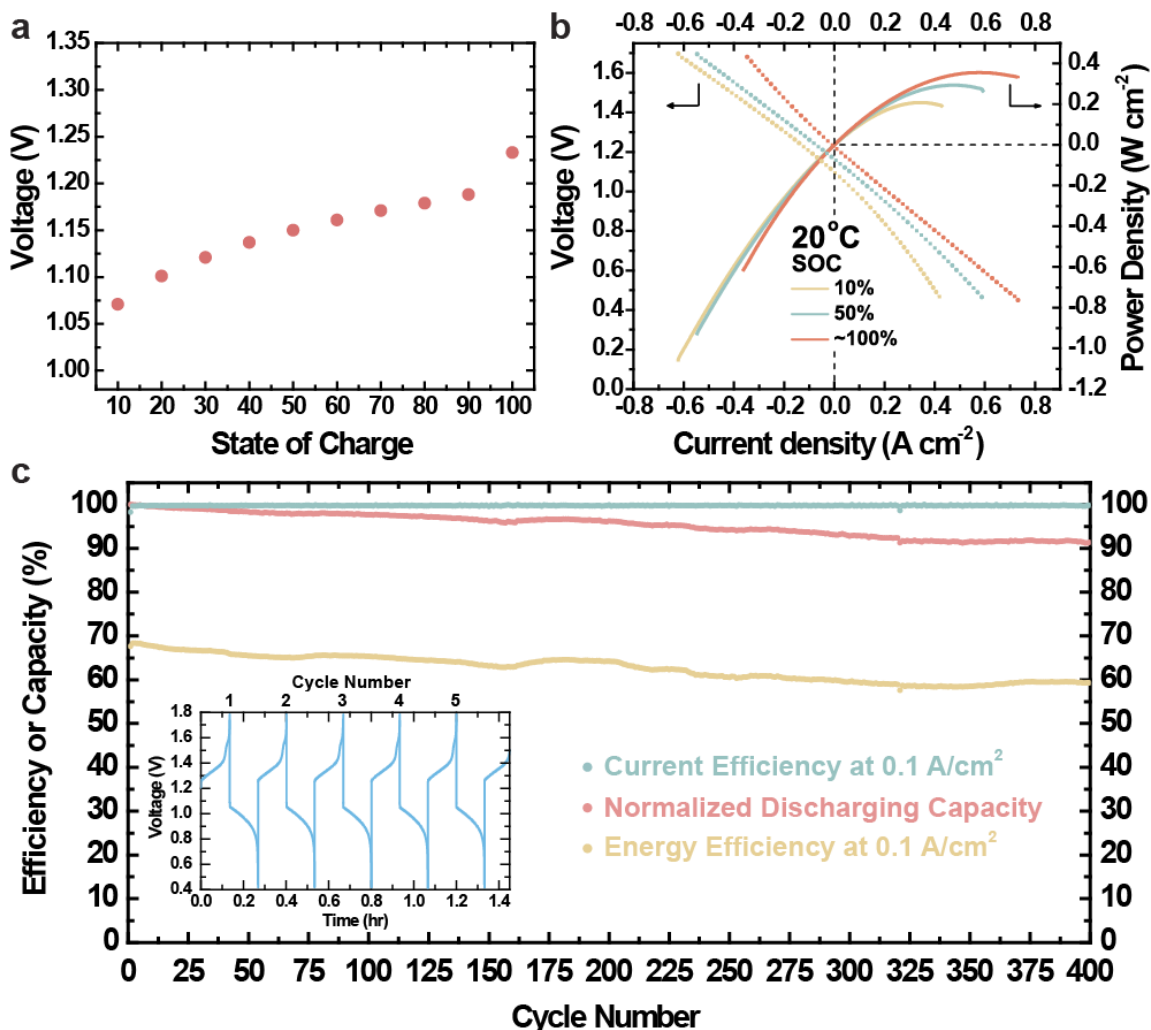
379 The authors declare no competing financial interests.



380

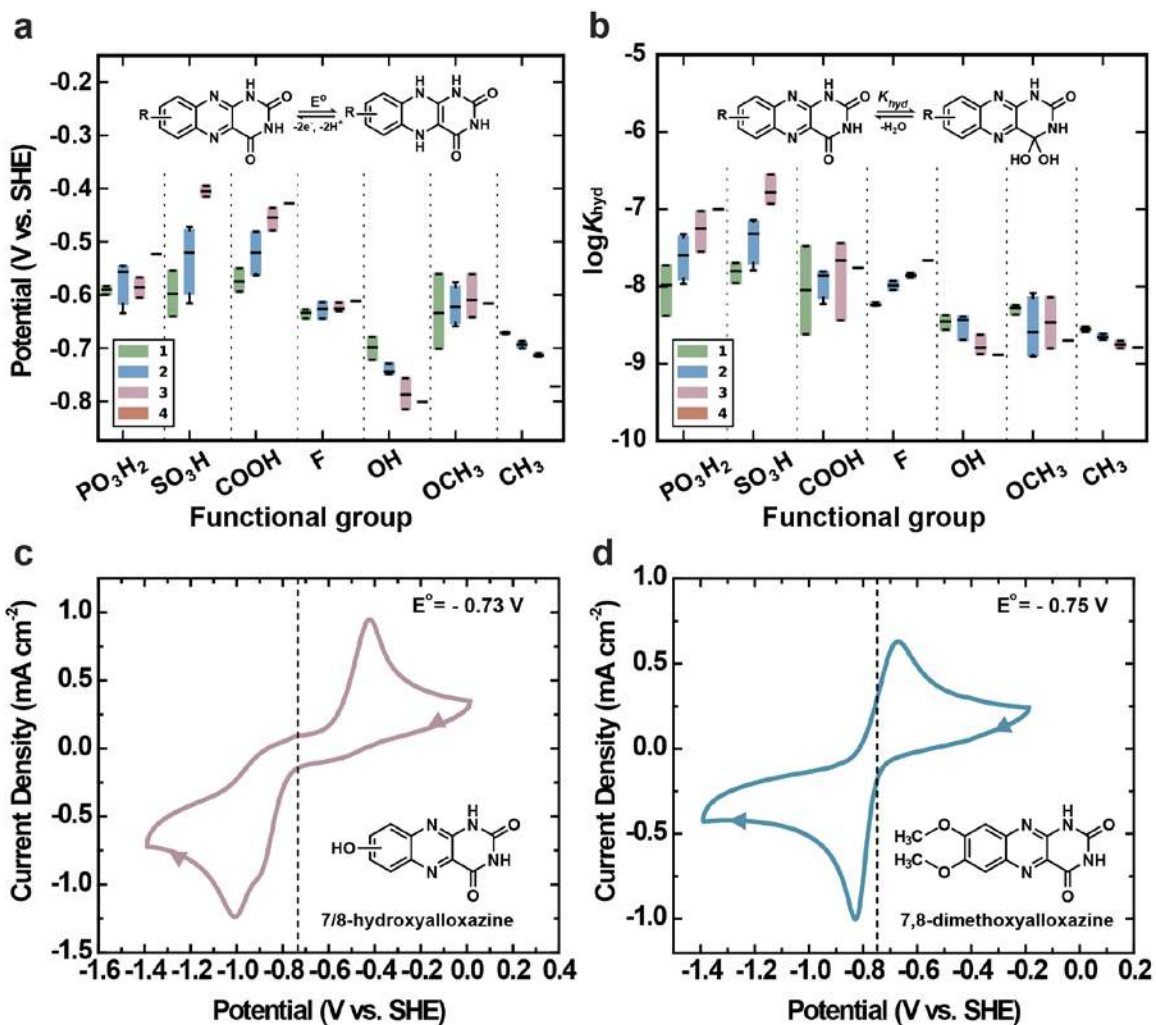
381 **Figure 1 | Cyclic Voltammogram and Cell Schematic.** **a** and **b**, Molecular structures
 382 and cyclic voltammogram of 2 mM riboflavin 5' phosphate (FMN) and lumichrome,
 383 respectively, scanned at 10 mV/s and 100 mV/s on glassy carbon electrode. **c**, Cyclic
 384 voltammogram of 2 mM alloxazine 7/8-carboxylic acid (ACA) (red curve) and
 385 ferrocyanide (gold curve) scanned at 100 mV/s on glassy carbon electrode; arrows
 386 indicate scan direction. **d**, Schematic of cell in discharge mode. Grey arrow indicate flow
 387 direction of electrons and white arrows indicate electrolyte solution flow. Blue arrow
 388 indicates migration of cations across the membrane. Essential components of
 389 electrochemical cells are labeled with color-coded lines and text.

390



391
 392 **Figure 2 | Cell Performance** (a) Cell open-circuit voltage (OCV) vs. state-of-charge
 393 (SOC). All potentials were taken when the cell voltage stabilized to within ± 1 mV. 100%
 394 SOC was reached by a potentiostatic hold at 1.5 V until the current decreased to below
 395 5 mA/cm². (b) Cell voltage & power density vs. current density at 20 °C, at 10%, 50%,
 396 and ~100% SOC. Electrolyte composition: 0.5 M ACA and 0.4 M ferrocyanide + 40 mM
 397 ferricyanide were used in negative electrolyte and positive electrolyte, respectively. (c)
 398 Capacity retention, current efficiency and energy efficiency values over 400 cycles at 0.1
 399 A/cm². The normalized discharging capacity is evaluated based on the capacity of the
 400 first discharge cycle. (Inset: Representative voltage vs. time curves during 400 charge-
 401 discharge cycles at 0.1 A/cm², recorded between the 1st and 5th cycles.)

402

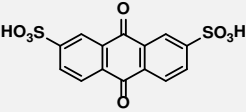
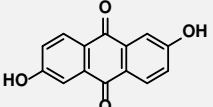
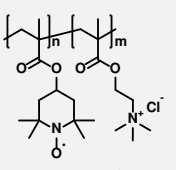
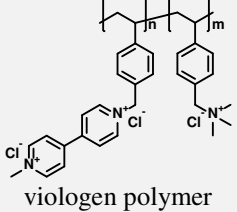
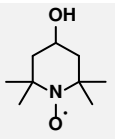
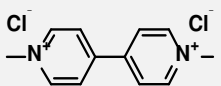


403

404 **Figure 3 | Theoretical Calculation and Cyclic Voltammetry of alloxazines.** (a)
 405 Predicted reduction potential at the B3LYP 6-311+G** CPCM level of theory for
 406 substituted alloxazines at pH=14.0 vs. RHE as a function of number and type of
 407 substituent. (b) Predicted logK_{hyd} at the B3LYP 6-311+G** CPCM level of theory for
 408 substituted alloxazines as a function of number and type of substituent. The bars
 409 represent the statistical distribution of predictions of all the possible substituted
 410 molecules with the given number of substituted sites. The bottom and top of the bar are
 411 the first and third quartiles, and the band inside the box is the median. The lines
 412 extending vertically from the boxes indicate the maximum and minimum of the range. (c)
 413 and (d) Molecular structures and cyclic voltammogram of 1 mM 7/8-hydroxyalloxazine
 414 and 7,8-dimethoxyalloxazine, respectively, scanned at 100 mV/s on glassy carbon
 415 electrode.

416

417 **Table 1 | High Performance Organic-based Aqueous Redox Flow Batteries.** This
 418 table focuses primarily on comparing molecular structures of redox-active organic
 419 molecules and evaluating their electrochemical stability based on capacity retention.

Positive Electrolyte	Negative Electrolyte	No. of Cycles (Condition)	Capacity Retention per Cycle (%) ^a	Energy Density (Wh/L)	Voltage (V)	Year of Publication	Merit (limitation)
bromine/ hydrobromic acid	 anthraquinone-2,7-disulfonic acid	10	99	16	0.86	2014 ⁸	Low cost and high performance (toxic bromine)
	750	99.84	16	2014 ⁹			
ferrocyanide	 2,6-dihydroxy-anthraquinone	100	99.1	6.8	1.2	2015 ¹⁰	Non-toxic and less corrosive electrolyte (reduced ion conductivity w.r.t. proton)
 TEMPO polymer	 viologen polymer	100	~ 99.75 ^b	10	1.15	2015 ¹¹	Cheap dialysis membrane (high electrolyte viscosity)
		10,000 (non-flow cell)	> 99.99				
 4-hydroxy-TEMPO	 methyl viologen	100 (low conc.)	> 99.99	8.4	1.25	2015 ¹³	Low cost all-organic electrolyte (low current density)
		100 (high conc.)	99.89				

420 ^a Capacity retention per cycle was derived from total capacity retention divided by total number of charge-
 421 discharge cycles.

422 ^b The capacity retention value was estimated based on the capacity retention vs. cycle number graph in
 423 figure 4 from reference 11.

424 **Table 2 | Reaction Scheme and Summary of Alloxazine Synthesis from Literature.**
 425 Alloxazines with different functional groups (-R) can be prepared by coupling *o*-
 426 phenylenediamine derivatives with alloxane in the presence of acetic acid and boric acid.

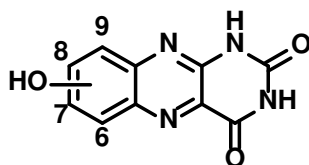
Rc1ccc(N)cc1N + O=C1NC(=O)C(=O)N1 $\xrightarrow[\text{boric acid}]{\text{acetic acid}}$ Rc1ccc2nc3c(nc2=1)C(=O)N3

o-phenylenediamine **alloxane** **alloxazines**

o-phenylenediamine	alloxazines	Reaction Time (h)	Yield (%)	Reference
	 alloxazine	2	87	Chen <i>et al.</i> ¹⁴
			95	Gonzalo <i>et al.</i> ¹⁵
	 lumichrome	2	95	Chen <i>et al.</i> ¹⁴
	 alloxazine 7/8-carboxylic acid (ACA)	3	100	Linden <i>et al.</i> ¹⁶
			95	<i>This work</i>
	 7/8-hydroxyalloxazine	3	86	<i>This work</i>
	 7,8-dimethoxyalloxazine	2	89	Chen <i>et al.</i> ¹⁴
			94	<i>This work</i>

427

428 **Table 3 | Theoretical Calculation and Substitution Patterns of Alloxazines.** Predicted
 429 standard reduction potential (E°) and logarithmic hydration equilibrium constant ($\log K_{\text{hyd}}$)
 430 for alloxazines with hydroxyl functional group(s).



hydroxylated alloxazines

431

432

433

434

435

436

437

438

439

440

441

442

443

444

No.	Position (-OH)				B3LYP 6-311+G** CPCM	
	6	7	8	9	E° (V)	$\log K_{\text{hyd}}$
1 Substituent						
1	H	H	H	-OH	-0.69	-8.4
2	H	H	-OH	H	-0.72	-8.7
3	H	-OH	H	H	-0.68	-8.5
4	-OH	H	H	H	-0.77	-8.3
2 Substituents						
5	-OH	-OH	H	H	-0.75	-8.4
6	-OH	H	-OH	H	-0.71	-8.6
7	-OH	H	H	-OH	-0.77	-8.2
8	H	-OH	-OH	H	-0.76	-9.3
9	H	-OH	H	-OH	-0.68	-8.4
10	H	H	-OH	-OH	-0.73	-8.7
3 Substituents						
11	-OH	-OH	-OH	H	-0.81	-8.9
12	-OH	-OH	H	-OH	-0.74	-8.3
13	-OH	H	-OH	-OH	-0.82	-8.7
14	H	-OH	-OH	-OH	-0.74	-8.9
4 Substituents						
15	-OH	-OH	-OH	-OH	-0.80	-8.9

A redox flow battery with an alloxazine-based organic electrolyte

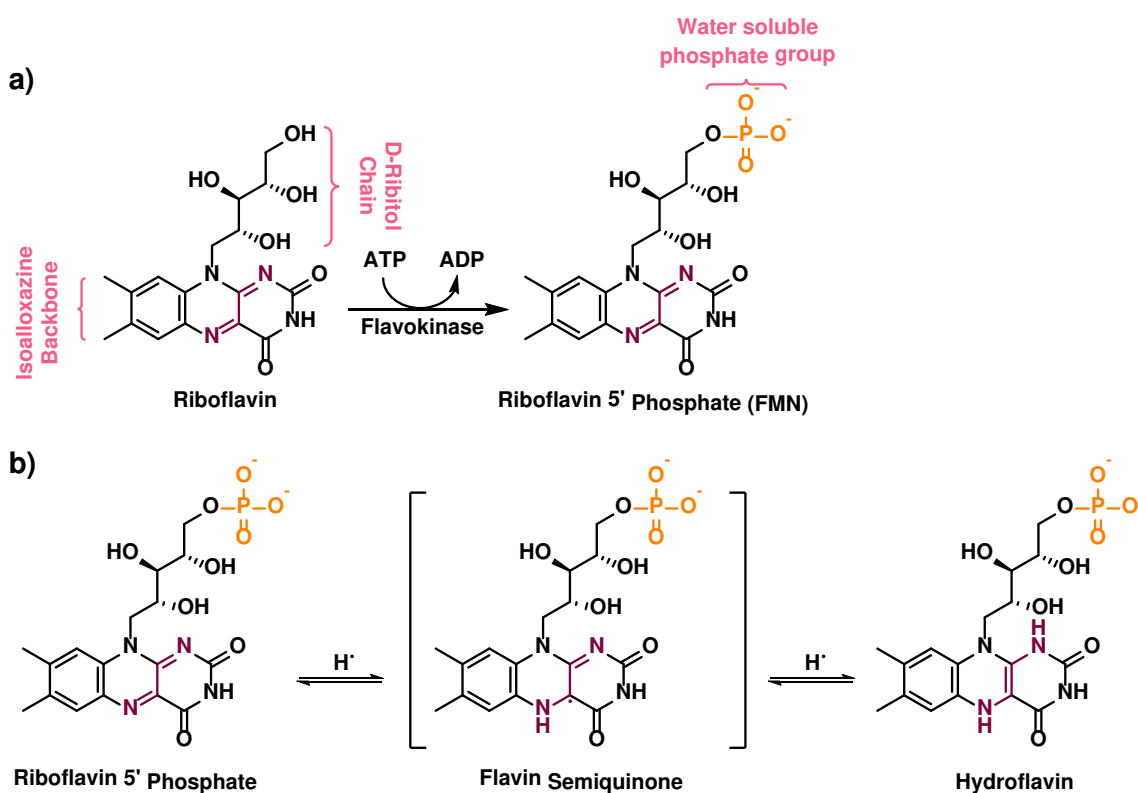
Kaixiang Lin¹, Rafael Gómez-Bombarelli¹, Eugene S. Beh^{1,2}, Liuchuan Tong¹, Qing Chen², Alvaro Valle³, Alán Aspuru-Guzik¹, Roy G. Gordon^{1,2*}, Michael J. Aziz^{2*}

¹Department of Chemistry and Chemical Biology, Harvard University, 12 Oxford Street, Cambridge, Massachusetts 02138, USA.

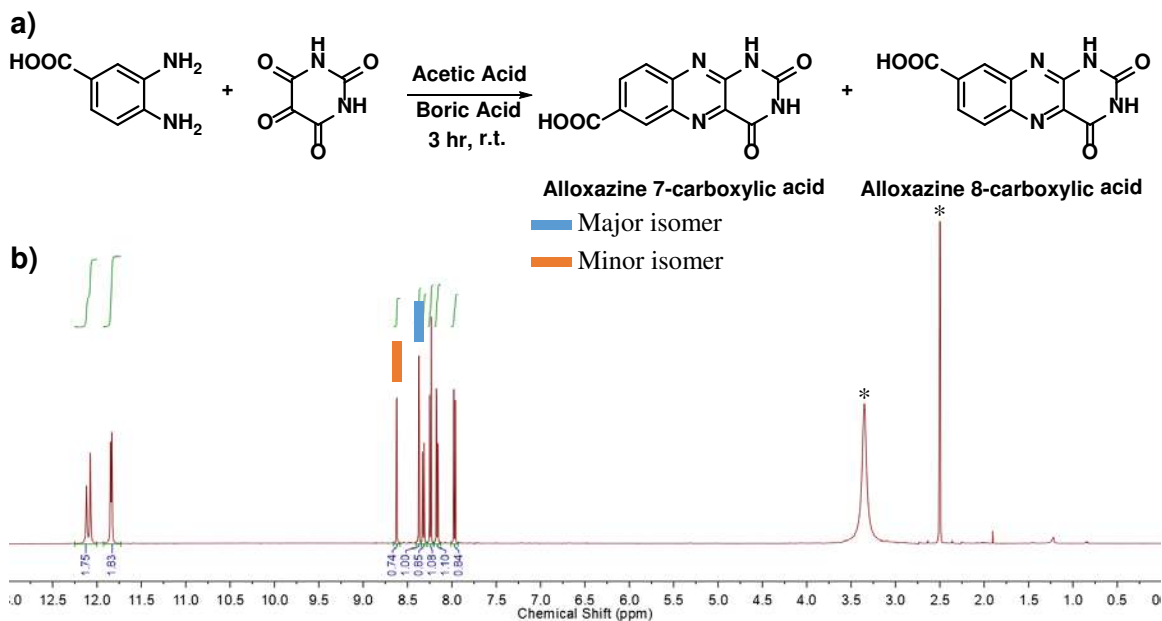
²Harvard John A. Paulson School of Engineering and Applied Sciences, 29 Oxford Street, Cambridge, Massachusetts 02138, USA.

³Harvard College, Cambridge, Massachusetts 02138, USA

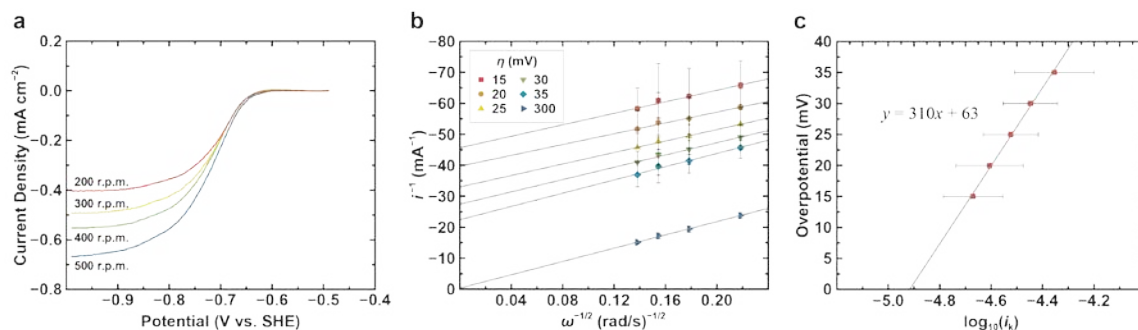
*Correspondence to: RGG (gordon@chemistry.harvard.edu) and MJA (aziz@seas.harvard.edu)



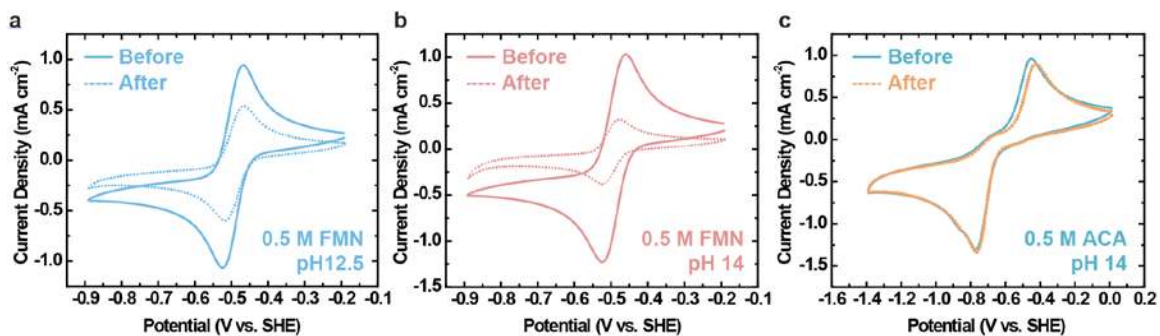
Supplementary Figure 1. (a) Biosynthesis of riboflavin 5' phosphate (FMN) from riboflavin (vitamin B₂). (b) Stepwise reduction of FMN into hydroflavin.¹⁸



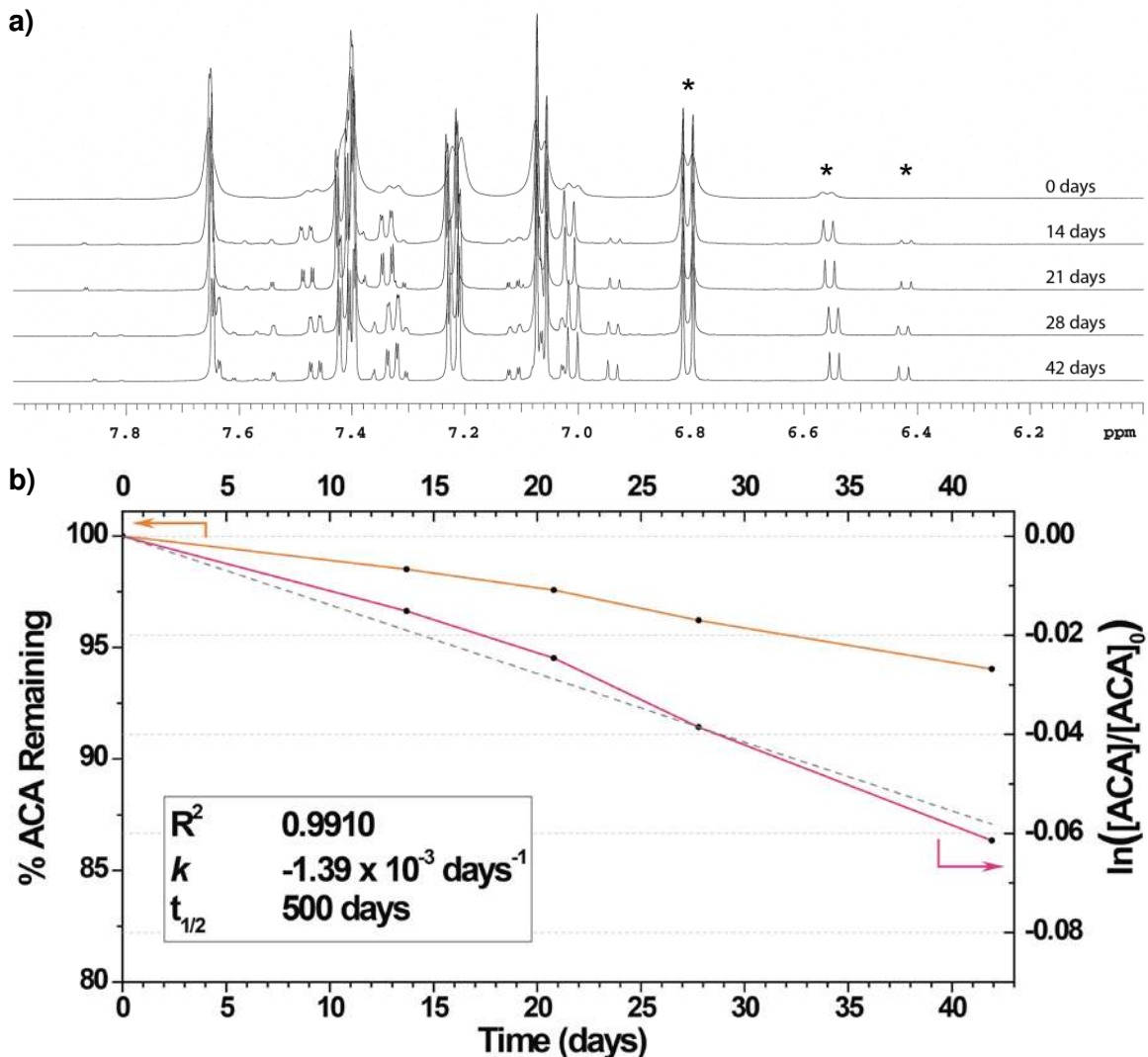
Supplementary Figure 2. (a) Synthetic scheme of alloxazine 7/8-carboxylic acid. **(b)** ^1H NMR (500 MHz, DMSO-d_6) spectrum of alloxazine 7/8-carboxylic acid. Major isomer: δ 12.02 (s, 1H), 11.79 (s, 1H), 8.29 (d, $J = 1.9$ Hz, 1H), 8.18 (d, $J = 8.8$ Hz, 1H), 8.09 (dd, $J = 1.9, 8.8$ Hz, 1H). Minor isomer: δ 12.06 (s, 1H), 11.80 (s, 1H), 8.55 (d, $J = 2.0$ Hz, 1H), 8.25 (dd, $J = 2.0, 8.8$ Hz, 1H), 7.90 (d, $J = 8.8$ Hz, 1H). Solvent peaks are labeled with asterisks. Final yield: 95%.



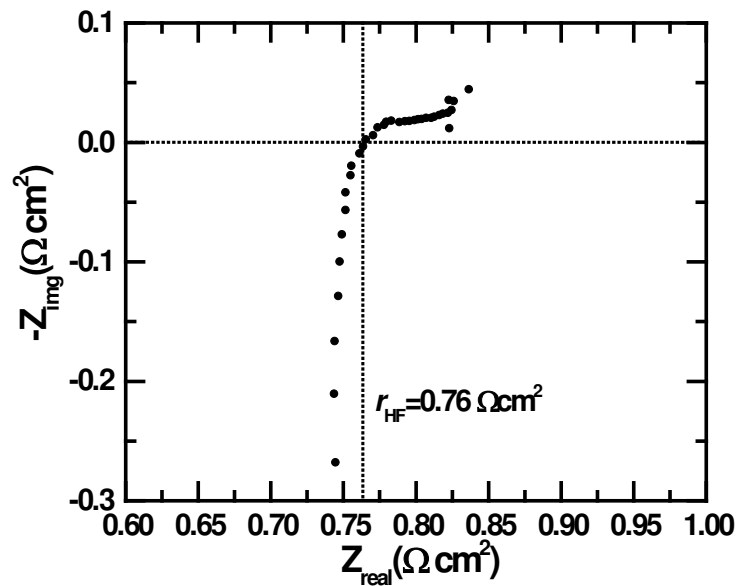
Supplementary Figure 3. (a) Plot of potential versus current density at different rotation rates of the RDE. The solution is 2 mM ACA in 1 M aqueous KOH, using a rotating disk electrode (RDE) of glassy carbon. Rotation rates are indicated. (b) Koutecký-Levich plot (i^{-1} versus $\omega^{-1/2}$) of 2 mM ACA in 1 M aqueous KOH. The current response, i^{-1} , is shown for six different ACA reduction overpotentials η . (c) Fit of RDE experimental data to the Tafel equation constructed using the current response in the absence of mass transport limitations at low ACA reduction potentials; i_k is the current extrapolated from the zero-intercept of the fitted lines in (b) (i.e. at infinite rotation rate). The line of best fit has the equation $y = 310x + 63$, from which $\alpha = 0.47(4)$ and $k_0 = 1.2(2) \times 10^{-5} \text{ cm s}^{-1}$ were calculated. Data are averaged over three runs; the numbers reported in parentheses indicate the standard deviation in the last reported digit.



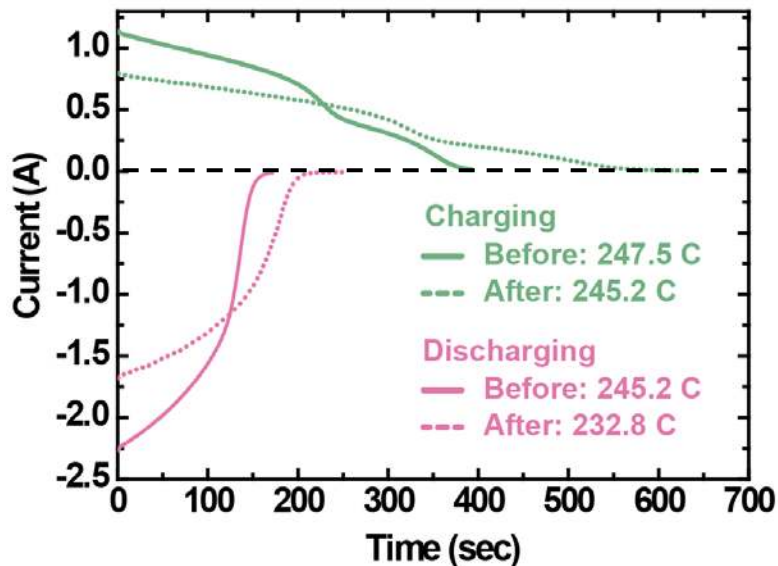
Supplementary Figure 4. (a) Cyclic voltammogram of $1/1000^{\text{th}}$ dilution of riboflavin 5' phosphate (FMN) at pH 12.5 before (solid line) and after (dotted line) 14 days, scanned at 100 mV/s on a glassy carbon electrode. (b) and (c) Cyclic voltammogram of $1/1000^{\text{th}}$ dilution of riboflavin 5' phosphate (FMN) and alloxazine 7/8-carboxylic acid (ACA), respectively, at pH 14 before (solid line) and after (dotted line) 14 days, scanned at 100 mV/s on a glassy carbon electrode.



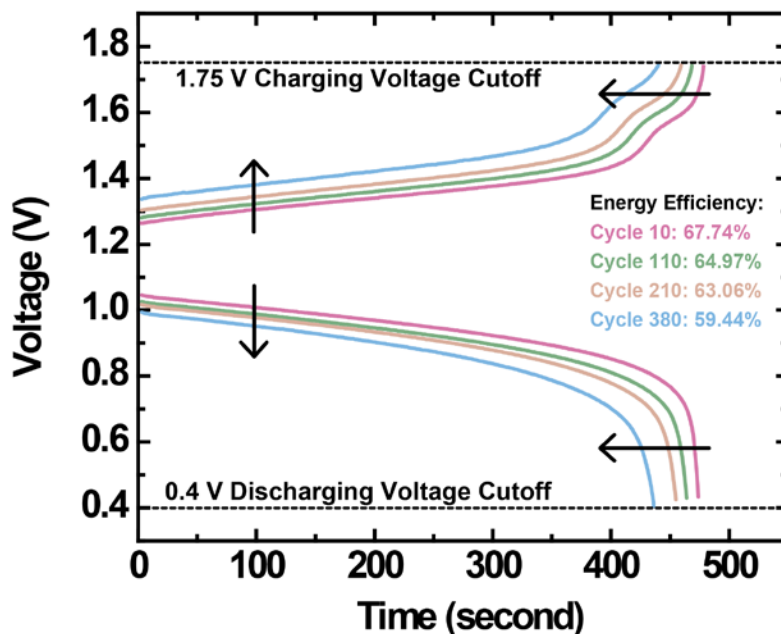
Supplementary Figure 5. ^1H NMR study of ACA stability in solution. (a) ^1H NMR spectra of a sample of 0.5 M ACA at pH 14 after various time points. The proportion of ACA that had decomposed was determined by comparing the area of the doublet that emerges at 6.43 ppm to the sum of the areas of the doublets at 6.55 ppm and 6.81 ppm, which come from the starting material. The peaks of interest are marked with a star. (b) Graphical depiction of the percentage of ACA remaining in the sample as a function of time (orange trace, left axis), as well as the same data replotted assuming first-order kinetics (pink trace, right axis). The gray dashed line represents the least-squares linear fit to the data in the pink trace.



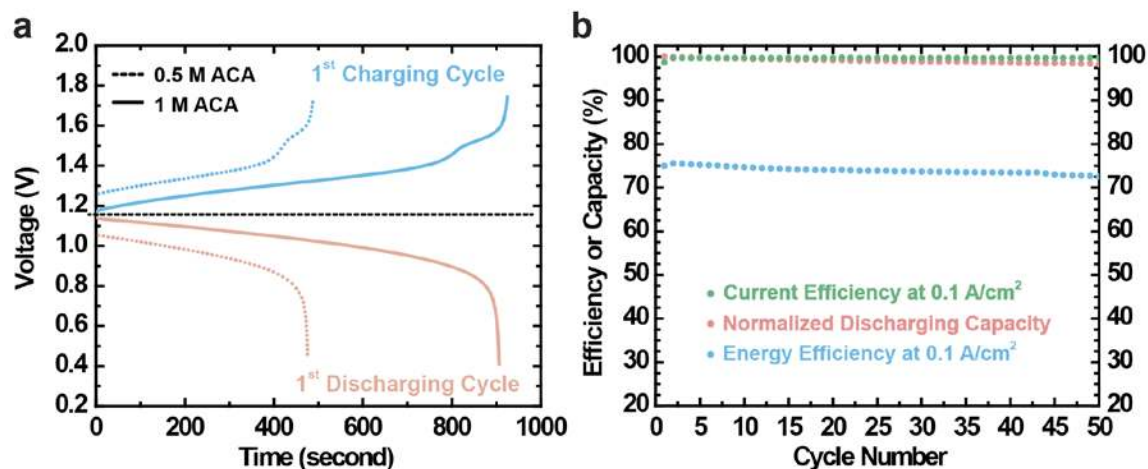
Supplementary Figure 6. Electrochemical impedance spectroscopy (EIS) of the ACA-ferrocyanide cell discussed in **Fig. 3a and 3b**. The EIS data were captured at 50% SOC. A high-frequency ASR (r_{HF}) was taken at ~ 80 kHz to be $0.76 \Omega \text{ cm}^2$. This comprises the membrane ionic resistance, the electrode electronic resistances, and the contact resistances, but not the electrolyte resistances. As the sum of the cell contact resistance and the electrode electronic resistance was previously measured in a dry-cell (a setup identical to the flow cell, but without the membrane and the flowing electrolyte) to be $\sim 0.02 \Omega \text{ cm}^2$, the membrane resistance, by subtraction, is thus $\sim 0.74 \Omega \text{ cm}^2$.



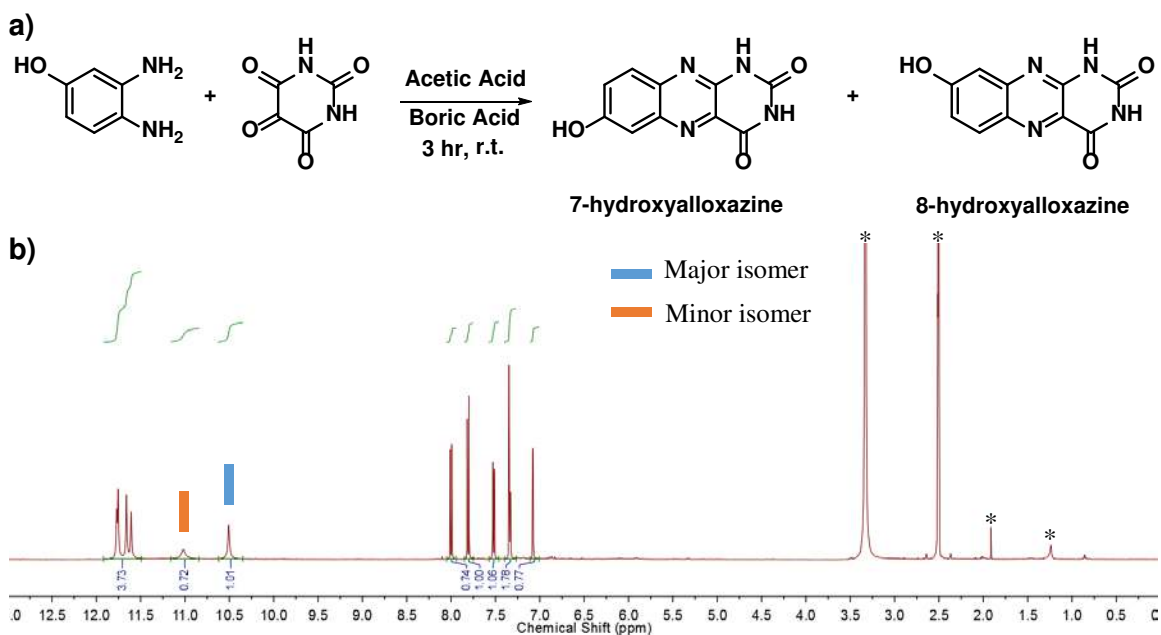
Supplementary Figure 7. Chronoamperometric (constant voltage) charging and discharging of ACA before (solid line) and after (dotted line) the 400 cyclic charge-discharge study. Black dashed line indicates zero current. Integration of the curves gives a 95% discharge capacity retention after 400 cycles.



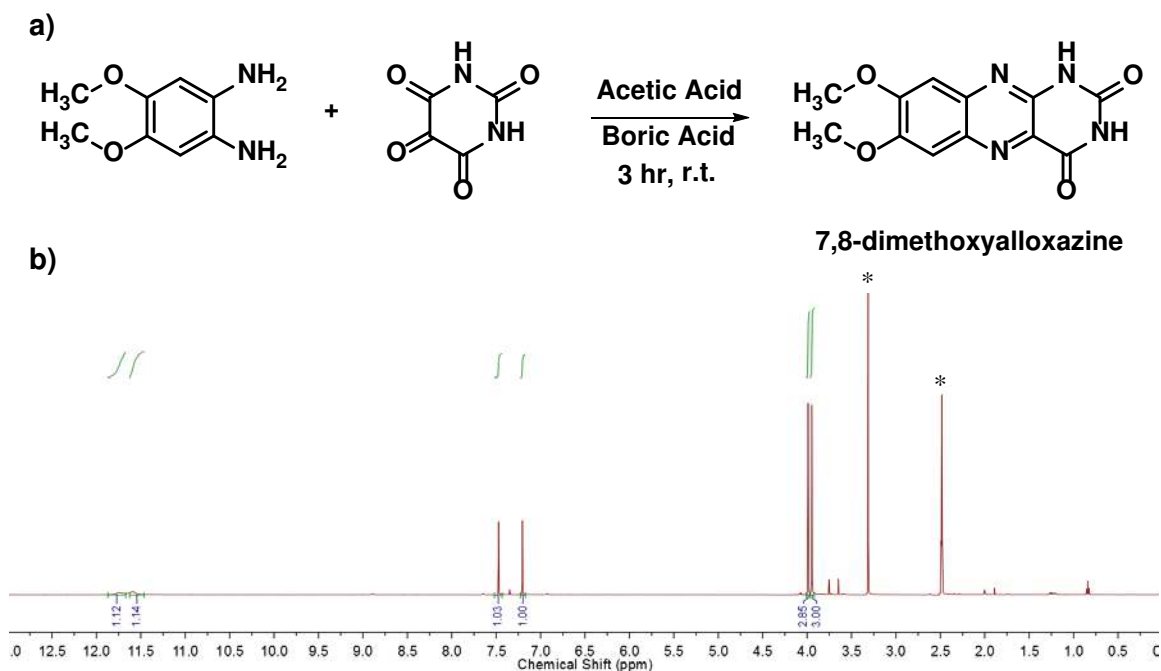
Supplementary Figure 8. Charging and discharge profiles of ACA at cycle no. 10, 110, 210 and 380 in the 400-cycle charge-discharge study. Black dashed lines indicate the voltage cutoffs. Black arrows represent the shifting directions of the curves during the course of the cycling study.



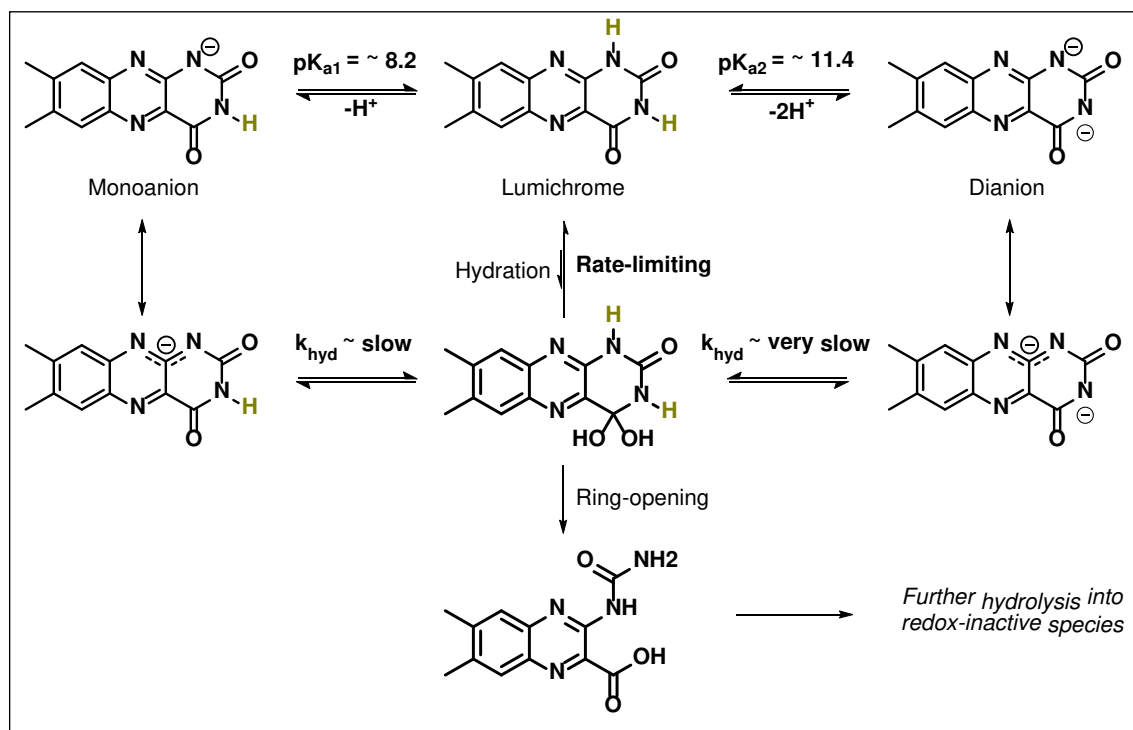
Supplementary Figure 9. (a) Representative voltage vs. time curves of the 1st charge-discharge cycle at 0.1 A/cm² for 0.5 M ACA (dotted line) and 1 M ACA (solid line) vs. 0.4 M ferrocyanide + 40 mM ferricyanide. (b) Capacity retention (97.5%), current efficiency (99.7%) and energy efficiency (74%) values measured over 50 charge-discharge cycles of the 1 M ACA negative electrolyte at 0.1 A/cm². Normalized discharging capacity is evaluated based on the capacity of the first discharge cycle.



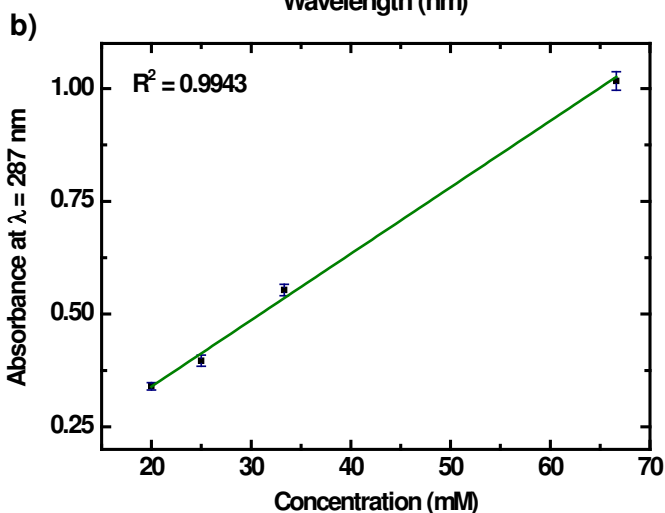
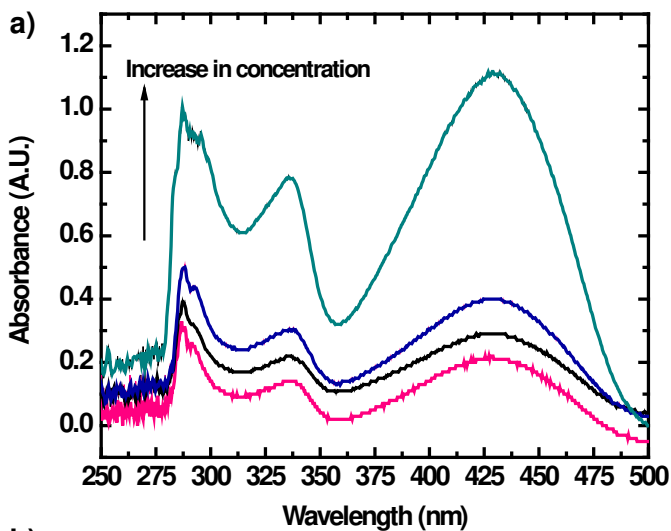
Supplementary Figure 10. (a) Synthetic scheme for 7/8-hydroxyalloxazine. (b) ^1H NMR (500 MHz, DMSO-d_6) spectrum of 7/8-hydroxyalloxazine. Major isomer: δ 12.02 (s, 1H), 11.79 (s, 1H), 8.29 (d, $J = 1.9$ Hz, 1H), 8.18 (d, $J = 8.8$ Hz, 1H), 8.09 (dd, $J = 1.9$, 8.8 Hz, 1H). Minor isomer: δ 12.06 (s, 1H), 11.80 (s, 1H), 8.55 (d, $J = 2.0$ Hz, 1H), 8.25 (dd, $J = 2.0$, 8.8 Hz, 1H), 7.90 (d, $J = 8.8$ Hz, 1H). Solvent peaks are labeled with asterisks. Final yield: 86%.



Supplementary Figure 11. (a) Synthetic scheme of 7,8-dimethoxyalloxazine. (b) ^1H NMR (500 MHz, DMSO-d_6) spectrum of 7,8-dimethoxyalloxazine δ 12.02 (s, 1H), 11.79 (s, 1H), 8.29 (d, $J = 1.9$ Hz, 1H), 8.18 (d, $J = 8.8$ Hz, 1H), 8.09 (dd, $J = 1.9$, 8.8 Hz, 1H). Solvent peaks are labeled with asterisks. Final yield: 94%.

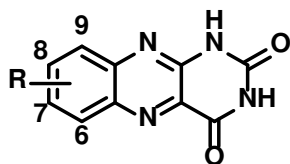


Supplementary Figure 12. Deprotonation, hydration and ring-opening reactions of lumichrome (7,8-dimethylalloxazine).²⁰



Supplementary Figure 13. (a) UV-Vis spectra of ACA at different concentration. (b) Standard calibration curve of ACA absorbance at $\lambda = 287$ nm vs. concentration. This calibration curve was interpolated to determine the concentration of ACA in diluted aliquots of a saturated solution, from which the saturation concentration of ACA was calculated.

Supplementary Table 1. Substitution patterns and predicted standard reduction potential (E°) and logarithmic hydration equilibrium constant ($\log K_{\text{hyd}}$) for alloxazines.



alloxazine derivatives

Position				B3LYP 6-311+G** CPCM											
6	7	8	9	E° (V)	$\log K_{\text{hyd}}$	E° (V)	$\log K_{\text{hyd}}$	E° (V)	$\log K_{\text{hyd}}$	E° (V)	$\log K_{\text{hyd}}$	E° (V)	$\log K_{\text{hyd}}$	E° (V)	$\log K_{\text{hyd}}$
1 substituent				R = -PO ₃ H ₂		R = -SO ₃ H		R = -COOH		R = -F		R = -OCH ₃		R = -CH ₃	
H	H	H	R	-0.62	-9.4	-0.67	-7.7	-0.53	-6.1	-0.63	-8.1	-0.54	-8.3	-0.67	-8.5
H	H	R	H	-0.57	-8.0	-0.52	-7.9	-0.56	-7.9	-0.66	-8.2	-0.71	-8.2	-0.68	-8.6
H	R	H	H	-0.59	-7.2	-0.57	-7.7	-0.60	-8.2	-0.64	-8.3	-0.70	-8.6	-0.67	-8.6
R	H	H	H	-0.59	-7.9	-0.63	-8.1	-0.59	-10.0	-0.63	-8.2	-0.57	-8.3	-0.67	-8.5
2 substituents															
R	R	H	H	-0.52	-9.0	-0.47	-9.4	-0.56	-8.2	-0.63	-8.0	-0.61	-7.7	-0.68	-8.6
R	H	R	H	-0.64	-7.7	-0.54	-7.8	-0.49	-10.4	-0.64	-8.1	-0.63	-8.9	-0.70	-8.8
R	H	H	R	-0.63	-7.3	-0.63	-7.4	-0.45	-7.8	-0.61	-7.9	-0.49	-8.1	-0.69	-8.6
H	R	R	H	-0.55	-7.3	-0.50	-7.2	-0.57	-7.9	-0.65	-8.0	-0.76	-8.3	-0.70	-8.7
H	R	H	R	-0.56	-7.5	-0.62	-7.1	-0.48	-7.8	-0.61	-7.9	-0.58	-9.2	-0.69	-8.7
H	H	R	R	-0.55	-8.0	-0.47	-7.0	-0.56	-7.7	-0.62	7.9	-0.66	-8.9	-0.69	-8.6
3 substituents															
R	R	R	H	-0.60	-7.4	-0.41	-6.9	-0.44	-7.9	-0.63	-7.9	-0.64	-8.1	-0.71	-8.6
R	R	H	R	-0.61	-7.1	-0.40	-7.1	-0.43	-7.4	-0.59	-7.8	-0.51	-8.2	-0.70	-8.7
R	H	R	R	-0.57	-8.2	-0.38	-6.1	-0.47	-10.1	-0.62	-7.8	-0.58	-8.8	-0.71	-8.9
H	R	R	R	-0.56	-6.8	-0.43	-6.7	-0.51	-7.4	-0.63	-7.9	-0.64	-8.9	-0.72	-8.8
4 substituents															
R	R	R	R	-0.52	-9.7	-0.35	-6.3	-0.43	-7.8	-0.61	-7.7	-0.62	-8.7	-0.77	-8.8

Supplementary Table 2. Predicted error in standard reduction potential (E^0) values for (iso)alloxazine molecules at pH = 7.4 and in logarithmic hydration equilibrium constant ($\log K_{\text{hyd}}$) values.

Method	E^0 (V)		$\log K_{\text{hyd}}$	
	R^2	Mean Error (meV)	R^2	Mean Error (log units)
PM7	0.86	23	0.79	1.5
PM7 COSMO	0.90	24	0.88	1.3
PBE 6-31G*	0.90	24	0.88	1.2
B3LYP 6-31G*	0.87	27	0.89	1.1
B3LYP 6-311+G**	0.89	25	0.85	1.2
B3LYP 6-311+G** CPCM	0.97	8	0.90	1.0